Andersson, B.-G. and Wannier, P.G. and Crawford, Ian (2002) Ultra-high-resolution observations of CH in southern molecular cloud envelopes. Monthly Notices of the Royal Astronomical Society 334 (2), pp. 327-337. ISSN 0035-8711.

Mon. Not. R. Astron. Soc. **334,** 327–337 (2002)

Ultra-high-resolution observations of CH in Southern Molecular Cloud envelopes

B-G. Andersson,[1]★ P. G. Wannier[2] and I. A. Crawford[3]

[1]*Center for Astrophysical Sciences, Johns Hopkins University, Baltimore, MD 21218, USA*
[2]*Jet Propulsion Laboratory, California Institute of Technology, Pasadena, CA 91109, USA*
[3]*Department of Physics and Astronomy, University College London, Gower Street, London WC1E 6BT*

Accepted 2002 February 27. Received 2002 February 25; in original form 2001 December 14

ABSTRACT

We present a mini-survey of ultrahigh-resolution spectroscopy (UHRS) of CH towards three southern molecular cloud envelopes. The sightlines are selected to probe physically similar gas in different Galactic environments. With a velocity resolution of $\sim 0.5\,\mathrm{km\,s^{-1}}$ ($R = 575\,000$) these observations resolve most kinematic components of the absorption lines. We do, however, detect one line component in the Lupus region, which is not resolved and for which an upper limit of $b < 0.3\,\mathrm{km\,s^{-1}}$ is found. We find a correlation between distance of the absorbing gas from the Galactic mid-plane and the fractional abundance of CH. We show that this correlation can be explained as being a result of a fall-off in the ultraviolet radiation field intensity and propose that CH observations in carefully selected sightlines might allow a mapping of the variations in the interstellar radiation field.

Key words: ISM: individual: Chamaeleon – ISM: individual: Lupus – ISM: individual: Southern Coalsack – ISM: molecules.

1 INTRODUCTION

Molecular clouds are known to be surrounded by lower-density envelopes, or haloes, where the gas goes from molecular to atomic form (e.g. Andersson & Wannier 1993; Chromey, Elmegreen & Elmegreen 1989). One of the most important transitions in these regions is that from molecular to atomic hydrogen, both because hydrogen is the dominant constituent of the clouds, but also because the line spectrum of the hydrogen molecule provides radiative shielding for other molecules (e.g. CO), as well as a sensitive probe to the state of the gas. Until the launch of the *Far Ultraviolet Spectroscopic Explorer* (*FUSE*) in 1999 June, the systematic study of this transition was severely hampered. Although the atomic component could be easily observed using its 21-cm transition, the molecular component could only be studied through tracer molecules such as CO. Pioneering, high-resolution measurements of H_2 were performed with the *Copernicus* satellite in the 1970s (e.g. Spitzer, Cochran & Hirshfeld 1974) and later by the Shuttle-borne IMAPS experiment (Jenkins & Peimbert 1997), but in both cases flux limitations meant that only the brightest far ultraviolet (FUV) targets could be observed and hence a target selection based on location relative to a given cloud and cloud envelope could not be achieved. With the advent of *FUSE* observations, systematic mapping of these transition regions has become feasible (Wannier et al., in preparation). However, as the spectral resolution of *FUSE* is only $R \sim 20\,000$, it cannot resolve closely spaced velocity components nor can it resolve spectral lines with b-values typical for the interstellar medium ($b \lesssim 2\,\mathrm{km\,s^{-1}}$). Unresolved multiple components, with differing excitation temperature, can cause severe problems in the interpretation of the H_2 spectra (Spitzer, Cochran & Hirshfeld 1974; Jenkins et al. 1989) and it is hence important to remove such ambiguities from the analysis. One method to remove ambiguities is to acquire ultrahigh-resolution spectroscopic observations of species that: (i) are thought to coexist with H_2 and (ii) can be observed with existing spectrographs. Probably the two best candidates for ground-based instruments are neutral potassium (K I) and the CH radical. For both observational and theoretical reasons we have chosen to concentrate on CH. Several earlier studies (Federman 1982; Danks, Federman & Lambert 1984; Mattila 1986) have shown that CH traces H_2. This is not surprising as CH is, chemically, closely related to H_2 through its formation reactions in interstellar clouds (Federman 1982; Viala 1986). CH can be readily observed either in the visual range at λ4300 or in the radio regime at 3.335 GHz (9 cm). As cm-wave observing is sensitive to extended regions (over the size of the telescope beam), the best match to the absorption-line data for H_2 is achieved through visual absorption-line observations.

Because of Λ doubling, the λ4300 line of the CH radical shows a double structure with a line separation of 0.0205 Å. The two components are located at 4300.303 and 4300.3235 Å with equal f-values of 5.06×10^{-3} (Black & van Dishoeck 1988).

★E-mail: bg@pha.jhu.edu

In cloud haloes and in translucent clouds typical excitation temperatures for H_2 are of the order 100 K (Wannier et al. 1999). For purely thermal broadening at these temperatures, the expected b-value for CH is 0.32 km s^{-1}. Hence a spectral resolution of that order is needed to resolve multiple components and to determine the line shape. At present, only two spectrographs provide such resolving power: the 'double-pass echelle' at the 2.7-m telescope of the McDonald Observatory and the ultrahigh-resolution facility (UHRF) at the Anglo- Australian Telescope.

An ultrahigh-resolution spectroscopy (UHRS) survey of CH towards 20 stars ($R = 530\,000$) has been presented by Crane et al. (1995). These authors concentrated on the global properties of the CH absorption and did not place a strong emphasis of the relation between the sightlines and the geometry of the molecular clouds. An additional, limited, number of individual sightlines have also been observed (e.g. Crawford 1995).

We selected stars in three nearby southern molecular cloud haloes (Fig. 1); the Chamaeleon complex at $l \approx 300°$, $b = -13°$ to $-20°$ and a distance of $d = 160 \pm 20$ pc (Whittet et al. 1997); the Southern Coalsack at $l \approx 303°$, $b = -4°$ to $+2°$ and $d \approx 225 \pm 25$ pc (Seidensticker & Schmidt-Kaler 1989) and the Lupus complex at $l \approx 340°$, $b = +2°$ to $+20°$ and $d = 150 \pm 10$ pc

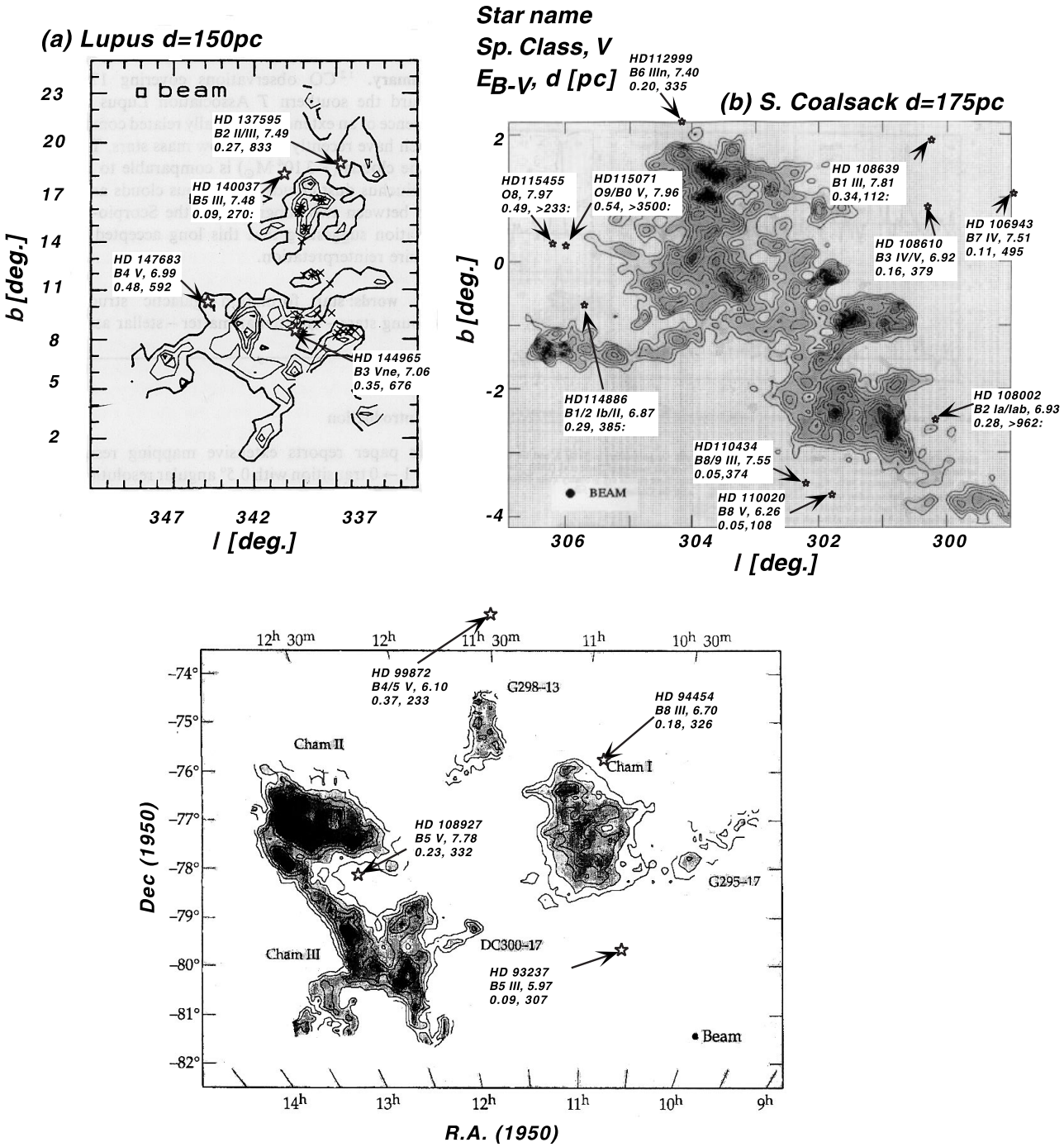

Figure 1. The UHRS target stars are plotted on CO ($J = 1-0$) maps. For each star some basic information is listed. Adapted (with permission from Astronomy and Astrophysics) from Murphy et al. (1986) for Lupus, Nyman et al. (1989) for the Southern Coalsack and Boulanger et al. (1998) for Chamaeleon.

(Crawford 2000). These clouds are all nearby, unaffected by violent star formation and span a range of distances from the Galactic mid-plane from 0 to 50 pc. The Lupus complex is, and the Southern Coalsack might be, associated with the Gould's belt structures (Crawford 1991). Because of their high Galactic latitudes, or in the case of the Southern Coalsack, extensive study, we can be relatively certain that the sightlines under study only intercept single cloud-complexes, hence locating the absorbing gas reliably in space. In Table 1 we summarize the most pertinent information on the stars/sightlines. In all but three cases the trigonometric and photometric parallaxes are consistent with each other. For HD 108639, 114886 and 140037, the photometric parallaxes are significantly larger than the trigonometric ones. For our purposes this is important in that it may signify errors in the spectral classification and hence in the intrinsic colours and colour excesses.

The Chamaeleon complex has been mapped in CO ($J = 1-0$) by Boulanger et al. (1998). It consists of three main condensations: Cham I, II and III together with the smaller cloud G298-13. The CO observations show the clouds to occupy a $v_{\rm LSR}$ range of about -1 to $+6\,{\rm km\,s^{-1}}$ with a velocity gradient running from the southeast (Cham III) towards the north and northwest. Observed linewidths for the CO emission are about $1-2.5\,{\rm km\,s^{-1}}$ (FWHM). Whittet et al. (1997) used spectroscopic and photometric data to derive distances to the subclouds in the range 140–180 pc. Their data show that little additional extinction exists, in these sightlines out to at least ~400 pc. Here we adopt a single distance of 160 ± 20 pc for the complex. Cham I has been mapped in polarization by several authors (Vrba, Marraco & Strom 1992; Whittet et al. 1994) and has been shown to be highly ordered over this cloud component.

The Southern Coalsack has been studied extensively at many wavelengths. Nyman, Bronfman & Thaddeus (1989) presented a fully sampled CO ($J = 1-0$) map of the cloud, but utilizing only a narrow velocity coverage between $v_{\rm LSR} \sim -10$ to $+8\,{\rm km\,s^{-1}}$. Bronfman et al. (1989) and Dame, Hartmann & Thaddeus (2001) have presented lower sampling-density maps, but with a wider velocity coverage showing additional CO emission at $v_{\rm LSR} \sim -50$ to $-25\,{\rm km\,s^{-1}}$ in, at least, the northern part of the cloud. While these components have kinematic distances characteristic of the Carina arm, we note that recent *FUSE* observations of H_2 in some Coalsack sightlines (Andersson, Shelton & Wannier 2001; Wannier et al., in preparation), show two velocity components consistent with the ~0 and $\sim -40\,{\rm km\,s^{-1}}$ CO emission. Cambrésy (1999) used star counts to map the large-scale extinction while Seidensticker & Schmidt-Kaler (1989) used four band photometric measurements, together with spectroscopic classifications of 284 stars to show that the cloud probably separates into two subclouds at ~175 and ~250 pc distance, but that no significant further extinction is present, either in the foreground or in the background this side of the Carina arm at ~1.3 kpc. Here we use a single distance of 225 ± 25 pc for our analysis. Andersson & Potter (in preparation) mapped the magnetic field of the cloud by measuring the polarization for the Seidensticker & Schmidt-Kaler (1989) stars. An ordered *B*-field is deduced.

The Lupus complex has been mapped in CO ($J = 1-0$) by Murphy, Cohen & May (1986) and in ^{13}CO ($J = 1-0$) by Tachihara et al. (1996). The cloud consists of a number of interconnected condensations as observed in, for example, ^{13}CO (Tachihara et al. 1996). Crawford (2000) observed Na I towards a number of sightlines in the direction of the cloud and using these

Table 1. Stellar data.

Star	$d_{\rm cloud}$ (pc)	Sp. class[a]	V (mag.)	$E(B-V)$ (mag.)	π^b (mas)	$d_{\rm star}$ (pc)	$\lvert z\rvert^c$ (pc)
Chamaeleon	160 ± 20						
HD 93237		B5 III	5.97	0.09	3.26 ± 0.48	307^{+53}_{-39}	51 ± 6
HD 94454		B8 III	6.70	0.18	3.07 ± 0.52	326^{+66}_{-47}	41 ± 5
HD 99872		B4/5 V	6.10	0.37	4.30 ± 0.81	233^{+54}_{-37}	29 ± 4
HD 108927		B5 V	7.78	0.23	3.01 ± 0.68	332^{+97}_{-61}	42 ± 5
Southern Coalsack	225 ± 25						
HD 106943		B7 IV	7.51	0.11	2.02 ± 0.72	495^{+274}_{-130}	4 ± 0.5
HD 108002		B2 Ia/ab	6.93	0.28	0.40 ± 0.64	>962	10 ± 1
HD 108610		B3 IV/V	6.92	0.16	2.64 ± 0.62	379^{+116}_{-72}	3 ± 0.4
HD 108639		B1 III[d]	7.81	0.34	8.9 ± 4.0[e]	112^{+92}_{-35}	8 ± 1
HD 110020		B8 V	6.26	0.05	9.23 ± 0.59	108^{+7}_{-7}	15 ± 2
HD 110434		B8/9 III	7.55	0.05	2.67 ± 0.75	374^{+146}_{-82}	14 ± 2
HD 112999		B6 III(n)	7.40	0.20	2.98 ± 0.73	335^{+109}_{-66}	9 ± 1
HD 114886		B1/2 Ib/II[d]	6.87	0.29	2.60 ± 0.47	385^{+95}_{-59}	3 ± 0.4
HD 115071		O9/B0 V	7.96	0.54	−0.63 ± 0.91	>3571	1 ± 0.1
HD 115455		O8	7.97	0.49	−0.2 ± 4.5[e]	>233	1 ± 0.1
Lupus	150 ± 10						
HD 137595		B2 II/III	7.49	0.27	1.20 ± 0.91	833^{+2615}_{-359}	48 ± 3
HD 140037		B5 III[d]	7.48	0.09	3.70 ± 0.96	270^{+95}_{-56}	46 ± 3
HD 144965		B3 Vne	7.06	0.35	1.48 ± 1.10	676^{+1956}_{-288}	22 ± 2
HD 147683		B4 V	6.99	0.48	1.69 ± 0.95	592^{+759}_{-213}	27 ± 2

[a] Houk & Cowley (1975); Houk (1978, 1982).
[b] *Hipparcos* measurements (Perryman et al. 1997), unless otherwise noted.
[c] Height above the Galactic mid-plane of the intersection of sightline and cloud.
[d] Trigonometric and photometric parallaxes are inconsistent.
[e] Tycho measurement (Høg et al. 2000).

data and *Hipparcos* distances, he derived a distance of 150 ± 10 pc. While he finds evidence for both approaching and receding velocity components caused by the Sco-Cen shell, the visual extinction associated with the shell is much lower [$E(B-V) \sim 0.03$ mag] than that due to the Lupus cloud [$E(B-V) \sim 0.3$ mag]. Polarimetric observations have been carried out by Rizzo, Morras & Arnal (1998), who find that the relative uniformity of the polarization angles implies a stronger role for the magnetic field in the southern part of the complex ('Lupus 4'; cf. Schwartz 1977) than in the northern part ('Lupus 1')

2 OBSERVATIONS AND DATA REDUCTION

The present observations were obtained using the UHRF at the Anglo-Australian Telescope (Diego et al. 1995), over the nights of 2000 April 17–20, inclusive. The spectrograph was used in its '$R = 600\,000$' mode, and a measurement of the instrumental profile (using a stabilized He–Ne laser as a source) indicated that the actual resolving power was $R = 575\,000$ ($0.52\,\mathrm{km\,s^{-1}}$, FWHM). The detector was a Tectronix charge-coupled device (CCD) (1024×1024 24-μm pixels), and the readout speed was set to 'extra slow' (resulting in a rms readout noise of $2.3\,\mathrm{e^-\,pixel^{-1}}$). The spectrograph was used in conjunction with an image-slicer (Diego 1993), and the output was binned by a factor of 8 perpendicular to the dispersion direction in order to reduce the readout noise associated with the resulting broad spectrum. Wavelength calibration was performed by means of a Th–Ar lamp, and a quartz–halogen lamp was used to obtain flatfields. As these observations are highly susceptible to detector read-noise, the decision was made to forego the full ($R \sim 900\,000$) resolution of the spectrograph in order to be able to observe the full sample.

Table 2. Observation log.

Star	UT date	Exposures ($n \times s$)	ZA (deg)	Co-added S/N ratio (continuum)	Comment
HD 93237	17-4-2000	4×1800	49–51	95	Some cirrus
	20-4-2000	2×1800	49–51		Some cirrus
HD 94454	17-4-2000	4×1800	45–46	70	Some cirrus
	19-4-2000	2×1800	45		Clear
	20-4-2000	2×1800	45–46		Some cirrus
HD 99872	18-4-2000	3×1800	44–49	65	Cirrus
	20-4-2000	2×1800	41–42		Some cirrus
HD 108927	19-4-2000	3×1800	51–55	15	Clear
HD 106943	19-4-2000	2×1800	31–34	20	Clear
HD 108002	17-4-2000	4×1800	37–48	45	Cirrus
	19-4-2000	2×1800	45–51		Clear
	20-4-2000	1×1800	34–35		Some cirrus
HD 108610	18-4-2000	3×1800	31–33	15	Cirrus
HD 108639	19-4-2000	2×1800	30–34	25	Clear
HD 110020	17-4-2000	3×1800	35–37	35	Cirrus
HD 110434	19-4-2000	4×1800	35–36	40	Clear
	20-4-2000	2×1800	35		Some cirrus
HD 112999	18-4-2000	3×1800	34–43	10	Cirrus
HD 114886	17-4-2000	3×1800	43–53	15	Cirrus
HD 115071	18-4-2000	4×1800	36–49	35	Some cirrus
	19-4-2000	3×1800	32–38		Clear
	20-4-2000	2×1800	31–33		Some cirrus
HD 115455	18-4-2000	4×1800	31–36	15	Cirrus
	20-4-2000	2×1800	33–37		Some cirrus
HD 137595	18-4-2000	5×1800	23–51	25	Some cirrus
	20-4-2000	2×1800	2–14		Some cirrus
HD 140037	19-4-2000	2×1800	26–39	45	Clear
HD 144965	17-4-2000	3×1800	23–41	35	Cirrus
	20-4-2000	2×1800	10–19		Some cirrus
HD 147683	19-4-2000	2×1800	5–17	70	Clear
	20-4-2000	2×1800	15–28		Some cirrus

Except for the night of April 19, the observations were hampered by varying degrees of atmospheric cirrus cloud. This was particularly a problem during parts of the first two nights. As discussed below, we find that the photometry of targets observed at those times is uncertain, in the sense that non-target sources of detector counts seem to contribute significantly to the data, and hence the contrast in the derived spectra is decreased. Possible cloud-scattered light from the 97–100 per cent illuminated moon and a somewhat uncertain dark current are likely causes of these calibration difficulties. The problem was most severe for Southern Coalsack targets. We observed Chamaeleon sources at the beginning of the nights, followed by Coalsack targets and ending with Lupus stars. The right ascension (RA) of the Moon was similar to that of the Coalsack (RA $\sim 12^{\rm h}$), so the Moon was at its highest elevation (ZA $\sim 30°$) during the Coalsack exposures. The Chamaeleon observations were less affected as the cloud coverage generally developed later in the observing nights. The Lupus observations were also less affected, probably because, by the time we moved over to the Lupus target, the Moon had dropped to ZA ~ 55–$65°$.

For those targets that were only observed on April 17 or 18 and for which no line was detected, we therefore do not quote upper limits for the CH line, but simply note them as non-detections. Details of the observations are given in Table 2.

After standard CCD calibration procedures (bias subtraction and flat-fielding) and cosmic ray removal, extraction of the one-dimensional spectra was performed using the IRAF package DOSLIT. Because we were using the image-slicer, which maps different slices of the stellar image to different positions along the slit, we also used the LONGSLIT extraction routines to check for possible alignment effects of the echelle order with the CCD rows. We find no significant difference in the derived spectra using the two methods.

3 ANALYSIS

After extracting the spectra we fit single- or multiple-velocity components to the CH profiles as warranted. We used a non-linear fitting procedure (implemented in IDL) which explicitly imposed the two Λ-doubling components as well as performing a convolution with the instrumental resolution (assumed to be a Gaussian of FWHM $0.52\,{\rm km\,s^{-1}}$). We assumed equal populations in the two Λ-doublet components and quote equivalent widths and column densities for the sum of the two components. For the sightlines where unambiguous detections were made the measured equivalent widths are quoted in Table 3 with uncertainties derived from propagation of errors from the uncertainties in the fitting parameters.

For those sources where no line was detected, we estimated upper limits to the equivalent widths following Morton, York & Jenkins (1986),

$$\epsilon_{\rm W} = 2 \times \delta\lambda\sqrt{M}/(S/N), \qquad (1)$$

where $M \approx \sqrt{4\Delta\lambda_{\rm I}^2 + \Delta\lambda_{\rm L}^2}/\delta\lambda$, $\delta\lambda$ is the pixel width, $\Delta\lambda_{\rm I}$ is the instrumental resolution (FWHM) and $\Delta\lambda_{\rm L}$ is the nominal width of the anticipated line. The calculated upper limits assume a conservative, nominal linewidth (FWHM) of $3.0\,{\rm km\,s^{-1}}$.

In the case of HD 147683 the fitted linewidth was narrower than the instrumental resolution. In this case we derived an upper limit to the linewidth by measuring χ^2 at a set of fixed b-values (letting the amplitude vary). For HD 115071 a similar procedure indicates

Table 3. Observational results and derived column densities.

Star	$v_{\rm LSR}$ ($\rm km\,s^{-1}$)	b ($\rm km\,s^{-1}$)	W^a (mÅ)	$N_{\rm CH}$ ($\times 10^{12}\,\rm cm^{-2}$)
Chamaeleon				
HD 93237	3.6 ± 0.5	0.7 ± 0.3	1.0 ± 0.2	1.2 ± 0.2
HD 94454	3.7 ± 0.1	1.6 ± 0.1	7.8 ± 0.8	9.4 ± 1.0
HD 99872	3.2 ± 0.1	1.7 ± 0.1	10.4 ± 0.6	12.6 ± 0.8
HD 109827	2.1 ± 0.1	0.7 ± 0.1	9.0 ± 3.8	10.8 ± 4.6
Southern Coalsack				
HD 106943	–	–	<2.6	–
HD 108002	1.7 ± 0.3	1.5 ± 0.3	2.6 ± 1.0	3.2 ± 1.2
HD 108610	–	–	<3.0	–
HD 108639	–	–	<2.0	–
HD 110020	–	–	<1.4	–
HD 110434	–	–	<1.4	–
HD 112999	–	–	–	–
HD 114886	–	–	–[b]	–
HD 115071	−3.5 ± 0.1	0.4 ± 0.1	2.0 ± 0.2	2.4 ± 0.2
	−3.2 ± 0.1	2.7 ± 0.1	4.8 ± 0.2	3.8 ± 0.2
HD 115455	−2.9 ± 0.2	3.6 ± 0.2	13.8 ± 1.2	17 ± 1
Lupus				
HD 137595	5.5 ± 0.3	3.5 ± 0.9	10.0 ± 2.4	12.2 ± 3.0
HD 140037	–	–	<0.5	–
HD 144965	4.7 ± 0.3	1.6 ± 0.3	11.8 ± 1.6	14.4 ± 2.0
HD 147683	5.3 ± 0.1	<0.3	1.6 ± 0.4	2.0 ± 0.4
	6.2 ± 0.1	1.9 ± 0.1	12.6 ± 0.8	15.2 ± 1.0
	11.6 ± 0.4	2.5 ± 0.6	4.2 ± 1.0	5.0 ± 1.2

[a] Upper limits are 2σ.
[b] Detected by (Gredel (1997) at $v_{\rm LSR} = -2.6$: $W = 4.5 \pm 0.5$ mÅ and $v_{\rm LSR} = -28.4$: $W = 3.5 \pm 0.5$ mÅ.

that the narrow line is marginally resolved and we can hence quote a measured *b*-value.

4 RESULTS AND DISCUSSION

4.1 Chamaeleon molecular cloud

We observed four stars in the region of the Chamaeleon clouds. The CH absorption in three of the sightlines occurs at $v_{\rm LSR} \sim 3.5\,{\rm km\,s^{-1}}$. In the fourth (HD 108927) the line is centred at $\sim 2.1\,{\rm km\,s^{-1}}$. These velocities are in good general agreement with those in the CO maps. Three of the sightlines, HD 93237, 99872 and 108927 are well fitted by single-velocity components. For HD 94454 a second component was considered as the observed spectrum shows inflection points in the absorption line. However, the best-fitting two-component fit is rejected because an F-test (Lupton 1993) shows that a second component is only justified at the 45 per cent level. The derived fit parameters are given in Table 3. Spectra with best-fitting models overplotted are shown in Fig. 2.

4.2 Southern Coalsack

We observed 10 stars in the Coalsack. Of these only two yielded clear detections (HD 108002 and 115071), while a third (HD 115455) shows a marginal detection (Fig. 3). HD 108002 shows a single component with $v_{\rm LSR} = 1.7\,{\rm km\,s^{-1}}$. For HD 115071 two velocity components might be warranted. A second component is only marginally justified from a statistical point of view (an F-test justifies the additional parameters at the 78 per cent level). As in the case of HD 147683 (see below) the fact that the spacing between the two very narrow absorption features exactly matches the Λ-doubling shift of CH, still makes the additional component very attractive. In this case the narrow component is marginally resolved and has a *b*-value of $0.4\,{\rm km\,s^{-1}}$. The two components are centred very close together at -3.5 and $-3.2\,{\rm km\,s^{-1}}$. A wide shallow component at $-2.5\,{\rm km\,s^{-1}}$ is measured for HD 115455. These centre velocities are in good agreement with the CO ($J = 1-0$) observations (Nyman et al. 1989). For HD 114886 we do not detect any CH absorption. Based solely on the counts in the continuum we would derive a 2σ upper limit to the CH absorption of 3.4 mÅ. However, Gredel (1997) detects CH at two velocities in this sightline with an equivalent width of W(CH; $v_{\rm LSR} = -2.6$) = 4.5 ± 0.5 mÅ and W(CH; $v_{\rm LSR} = -28.4$) = 3.5 ± 0.5 mÅ. As discussed above, we suspect that a significant fraction of the counts for this and other Coalsack stars observed under cloudy conditions are a result of scattered moonlight and hence the contrast in the derived spectra does not correspond to Poisson statistics.

We note that we do not detect the $-30\,{\rm km\,s^{-1}}$ component, seen by Gredel in HD 114886 in any of our Coalsack stars. Based on the map by Seidensticker & Schmidt-Kaler (1989) and the *FUSE* observations (Andersson et al. 2001) we would not expect such a component in the stars south of $b \sim -2°$, but for HD 115071, for example, where we do detect the $0\,{\rm km\,s^{-1}}$ component, we might expect it.

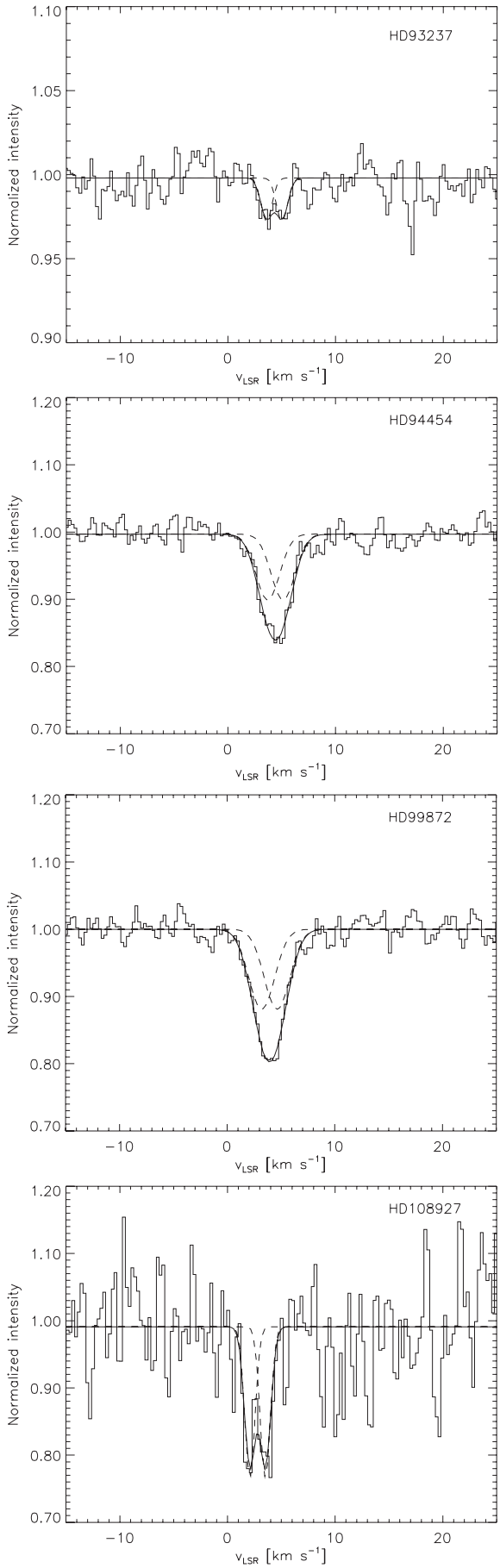

Figure 2. CH absorption-line spectra for the stars behind the Chamaeleon complex. For each star the best-fitting model is overplotted with a solid line and the two separate Λ-doubling components with a dashed line. In this and subsequent figures the velocity scale refers to the 4300.303-Å component.

4.3 Lupus molecular cloud

We observed four stars in the direction of the Lupus complex. Of these we detect CH in three (Fig. 4). The LSR velocities of CH in general agree well with those measured for CO ($J = 1–0$) (Murphy et al. 1986; Tachihara et al. 1996). In HD 137595 and 144965 single-component fits are satisfactory. In the HD 147683 sightline three velocity components are clearly justified. The narrowest component at $v_{\rm LSR} = 5.3\,{\rm km\,s^{-1}}$ is unresolved, and has a derived b-value of less than $0.3\,{\rm km\,s^{-1}}$. This is, to our knowledge, the narrowest interstellar CH absorption observed to date. This velocity width corresponds to pure thermal broadening for $\sim 100\,{\rm K}$ gas. While H_2 data towards similar sightlines do sometimes show temperatures somewhat below this value (Rachford et al. 2000), the fractional abundance of CH is expected to drop steeply towards the more opaque and presumably colder gas near the interior of the cloud. Hence further study of this sightline is warranted.

4.4 Fractional CH abundance

The CH radical has a fairly well-understood chemical network (Black & Dalgarno 1977; Federman 1982), with the primary formation mechanism from reactions of H_2 with C^+:

$$C^+ + H_2 \rightarrow CH_2^+ + h\nu \tag{2}$$

followed either directly by electron recombination or after

$$CH_2^+ + H_2 \rightarrow CH_3^+ + H \tag{3}$$

in both cases leading to CH formation. The destruction in diffuse gas is dominated by photodissociation through several channels (Sandell 1978) with a minor contribution from reactions with C^+. For low-extinction regions direct dissociation and photoionization dominate, while for higher-extinction gas, absorption at $\lambda 3134$ into the pre-dissociative $C^2\Sigma^+$ state dominates. In denser, more opaque gas, CH is also destroyed by reactions with atomic oxygen to form CO and HCO^+ (van Dishoeck & Black 1986). In diffuse gas we can hence write the steady-state abundance of CH (Federman 1982) as

$$x({\rm CH}) \approx \frac{\frac{2}{3}k_5 x(C^+) f}{\beta/n}, \tag{4}$$

where k_5 is the rate for reaction (2), f is the fractional abundance of H_2, β is the photodestruction rate and the factor of 2/3 is the branching ratio from CH_2^+ to CH. It is important to note here that, as there are several destruction mechanisms, the environment of the CH molecule is decisive for the chemical network. Hence, if we want to make detailed comparisons between different sightlines, we need to control this parameter as carefully as possible.

We can use data from the literature to estimate several of the parameters in (4). Based on recent *FUSE* data (Rachford et al. 2001, 2002) we estimate $f = 0.2–0.3$. We estimate a value for $k_5 = 5 \times 10^{-16}$ (Viala 1986) and further use the observations of Sofia, Fitzpatrick & Meyer (1998) to estimate the fractional abundance of C^+ in these sightlines to be of the order of 1×10^{-4}. Transforming the fractional abundance into the observable quantity $N({\rm CH})/E(B-V)$ we then find

$$\frac{N({\rm CH})}{E(B-V)} \approx 50\frac{n}{\beta}. \tag{5}$$

Finally, we can use the effective photodestruction rates for CH calculated by Sandell (1978) using the interstellar radiation field (ISRF) of Jura, Witt and Johnson (Jura 1974; Witt & Johnson 1973). We ask the question: is there a reasonable set of cloud parameters that will allow us to 'fit' the data? If we assume that the opacity characteristic of the photodestruction is similar to the line-of-sight one, $\tau_V \approx 0.8$ (cf. Sandell 1978, table 3), and a space density of $n \sim 50$, as observed for the B5 cloud envelope by Wannier et al. (1999), we derive $N({\rm CH})/E(B-V) \approx 3 \times 10^{13}\,{\rm cm^{-2}\,mag^{-1}}$. This value is in good agreement with our

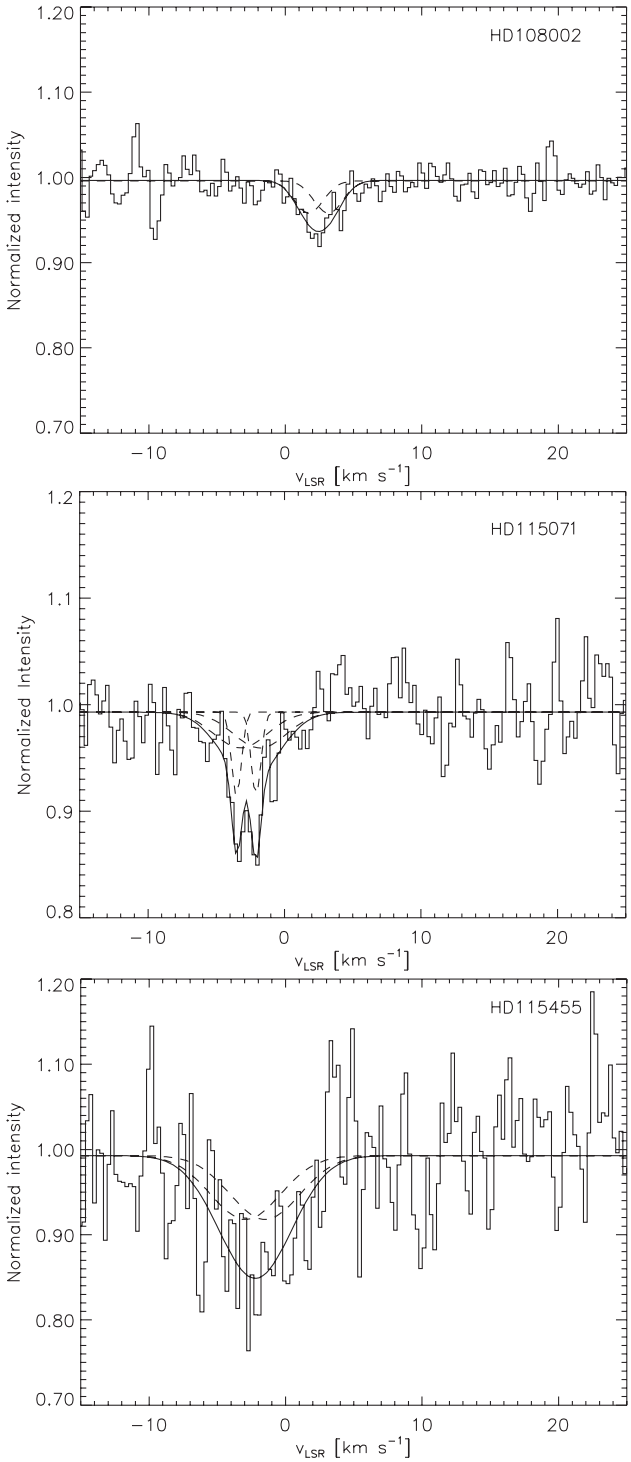

Figure 3. CH absorption-line spectra for the stars behind the Southern Coalsack. For each star the best-fitting model is overplotted with a solid line and the two separate Λ-doubling components with a dashed line.

measurements, given the uncertainties in n, β and $x(C^+)$. While this agreement might be fortuitous, all of the parameter values are reasonable and based on observational data. It is, however, clear that there is considerable uncertainty in the exact values of both the physical parameters and in the value of β.

It is worthwhile investigating the behaviour of the CH abundance as a function of Galactic environment. Our data set lends itself well to this particular study as: (i) the distances to the CH-bearing clouds and to the background stars are well known; (ii) the kinematic profiles, and hence the line-of-sight gas distributions, are simple and well resolved; and (iii) our sightlines were selected explicitly to probe a specific, common, physical environment in each of the clouds, namely the cloud envelopes. We used the measured colour excesses to transform the column densities to fractional abundances: $x(\mathrm{CH}) \propto N(\mathrm{CH})/E(B-V)$. While there is always a worry that dust associated with diffuse interstellar gas would contribute to the colour excess, the fact that our sightlines sample nearby, isolated clouds should minimize this potential problem. Some support for this comes from the various 'mappings' of colour excess as a function of distance cited above. In Fig. 5 we plot this measure of the fractional abundance as a function of the distance from the Galactic mid-plane of the absorbing gas. As has been shown by Savage et al. (1977) the transition from atomic to molecular hydrogen takes place at approximately a colour excess of 0.08. As the CH formation is primarily dependent on H_2, we have therefore excluded stars with $E(B-V) < 0.1$ from this plot. Similarly, we have marked sightlines with multiple detected kinematic components with open symbols in Fig. 5. For HD 115071 ($z \sim 0$ pc) and HD 147683 ($z \sim 27$ pc) these components are closely clustered in velocity space and hence we assume them to originate in physically related gas parcels. For these sightlines we have added the column densities of the components for the figure. For HD 114886 two widely separated components were detected by Gredel (1997). If the $-28\,\mathrm{km\,s^{-1}}$ component in his spectrum corresponds to Seidensticker's cloud α, then the two gas parcels are also physically related and the offset from the dense cloud to the sightline is similar. Under this assumption, we have also added the two components together for this sightline. Similar problems, only more pronounced, unfortunately apply to most other published CH measurements. Most of the sightlines reported by Crane et al. (1995) exhibit multiple-velocity components. In addition, many of their sightlines have poorly determined cloud distances, and hence pose problems in terms of the local gas environment. For most other data sets the spectral resolution of the data makes it impossible to say with confidence whether multiple components

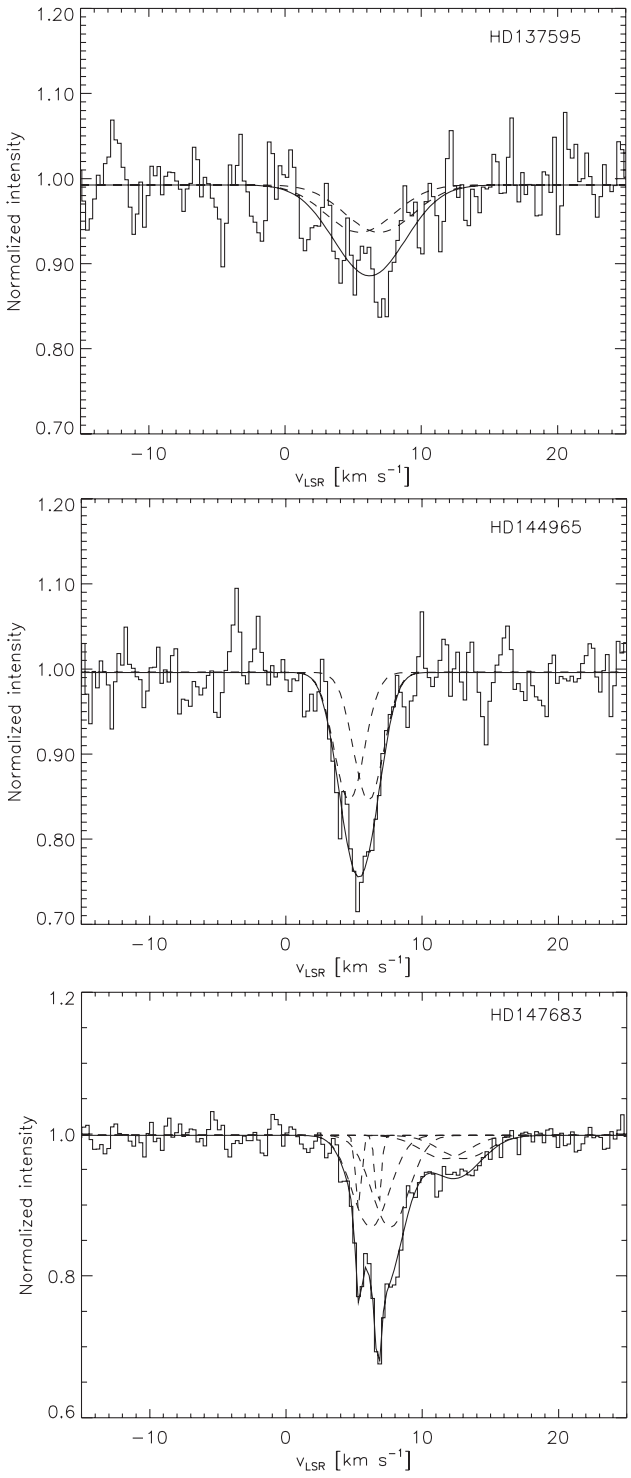

Figure 4. CH absorption-line spectra for the stars behind the Lupus complex. For each star the best-fitting model is overplotted with a solid line and the two separate Λ-doubling components with a dashed line.

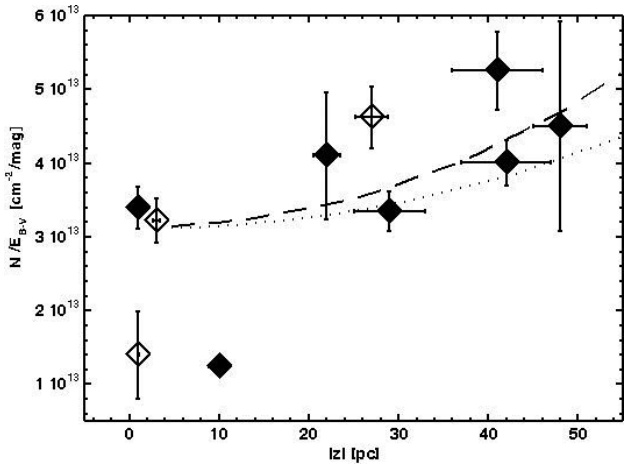

Figure 5. Fractional abundance of CH as a function of height above the Galactic plane. The dotted line represents a simple model of the ISRF described in Appendix A with a UV source scaleheight of ~50 pc and a dust scaleheight of ~200 pc. The dashed curve differs in that the dust scaleheight here is ~400 pc.

are present or not. In these cases we cannot determine either the distance from the Galactic mid-plane of the absorbing gas or the amount of colour excess attributable to the gas associated with each of the kinematic components. We have hence not attempted to include other data sets in the present analysis.

A weak, but discernable, trend is apparent in the fractional abundance of CH as a function of z. A Kendall rank-order test (Lupton 1993) of the data shows that the correlation is 2.6σ away from the null hypothesis, while if we remove the two lowest points, corresponding to HD 108002 and 115071, the null hypothesis is rejected at the 1.8σ level. The selection of the sources in our sample should: (i) make the CH formation rates comparable (by excluding sources with $E(B-V) < 0.1$) and (ii) place the absorbing gas at similar distances from the cloud surfaces (or equivalently at similar optical depths to the outside radiation field). Hence, the increase in the fractional CH abundance would seem to imply a general decrease in the Galactic diffuse radiation field with increasing distance from the mid-plane. To explore the possibility that carefully selected CH observations might be used to trace the variations in the ISRF we have developed a simple model for the ISRF as a function of distance to the Galactic plane (see Appendix A).

We have used this model, normalized to the field of Jura, Witt and Johnson (Jura 1974; Witt & Johnson 1973) at $z = 0$, together with equation (5) to predict the behaviour of x(CH) as a function of distance from the galactic mid-plane. We overplot the resulting predictions for two choices of parameters in Fig. 5. The models have been normalized to yield $N(\mathrm{CH})/E(B-V) \approx 3 \times 10^{13}\,\mathrm{cm^{-2}\,mag^{-1}}$ at $z = 0$ in concordance with the estimate above. The two models differ in the ratio of the emission (stellar) and absorption (dust) scaleheights. The implied scaleheight of ultraviolet (UV) sources from both models is ~ 50 pc, while the diffuse dust distribution is found to have a scaleheight of ~ 200 pc (dotted line) and ~ 400 pc (dashed line), respectively, for the two models. The value for the emissivity is consistent with the scaleheight of early-type (O) stars capable of producing photons causing direct photodissociation or photoionization (Mihalas & Binney 1981). The ISRF at the wavelength of the pre-dissociative excitation (λ3134) can be characterized by a diluted blackbody of $T_{\mathrm{eff}} = 7500$ K (Mezger et al. 1982) or roughly equivalent to a late A-type star. The scaleheight for such stars is ~ 120–190 pc (Mihalas & Binney 1981) and is hence larger than is implied by our CH results. The lower of the two scaleheights for the absorption is close to that observed for H I, while 400 pc is somewhat large for the interstellar medium (ISM).

Two caveats to the implied correlation are immediately clear. First, the dispersion in x(CH) for the low-z targets in the Coalsack is fairly large, while based on a limited number of sources. For HD 115071 the distance is also large and poorly known, making the distribution of extinction along the line of sight more uncertain. If the characteristic CH abundance at small values of z (in units of $N/E(B-V)$ is 3–$4 \times 10^{13}\,\mathrm{cm^{-2}\,mag^{-1}}$, rather than the 1–$3 \times 10^{13}\,\mathrm{cm^{-2}\,mag^{-1}}$ implied by the present results, the fit to the models would be much worse. Secondly, while Chamaeleon and Lupus sightlines overlap each other in $|z|$ (see Table 1) Lupus is associated with Gould's belt of early-type stars (Stothers & Frogel 1974; Crawford 2000) while Chamaeleon is not and hence if the Gould's belt stars contribute a significant fraction of the local UV photons, then the similarity of ISRF for the two complexes is in question. However, very few O-stars have been detected in the Sco-Cen OB association (de Geus, de Zeeuw & Lub 1989), which delineates Gould's belt in the direction of the Lupus cloud.

Given these uncertainties, the comparison between our observations and model is encouraging and shows that CH observations might possibly be used as a tracer of the ISRF, given the right source selection. Further ultrahigh-resolution observations of kinematically simple sightlines, particularly those transversing clouds at larger distances from the Galactic mid-plane are needed to test the validity of our model.

5 CONCLUSIONS

We have presented a mini-survey of ultrahigh-resolution spectroscopy of CH in the envelopes of three southern molecular clouds. The main results are as follows.

(i) Most sightlines show single kinematic components with b-values of around $1\,\mathrm{km\,s^{-1}}$, consistent with an origin in foreground molecular cloud envelopes.

(ii) In two sightlines we detect components at, or below, the resolution of our data ($0.3\,\mathrm{km\,s^{-1}}$). The narrowest of these correspond to purely thermal velocity broadening for 100 K gas and constitute the narrowest CH absorption line detected to date.

(iii) We find a weak, but significant, correlation of the fractional abundance of CH with height above (or below) the Galactic mid-plane (z). We suggest that the most likely cause of this correlation is a systematic drop-off in the strength of the ISRF with z. We developed a simple model of the ISRF that accounts for the observations.

ACKNOWLEDGMENTS

We thank PATT for the award of telescope time. IAC thanks PPARC for the award of an Advanced Fellowship. The work reported herein was, in part, carried out at the Jet Propulsion Laboratory, California Institute of Technology, under contract with the National Aeronautics and Space Administration.

REFERENCES

Andersson B-G., Wannier P. G., 1993, ApJ, 402, 585
Andersson B-G., Shelton R. L., Wannier P. G., 2001, BAAS, 33, 873
Black J. H., Dalgarno A., 1977, ApJS, 34, 405
Black J. H., van Dishoeck E. F., 1988, ApJ, 331, 986
Boulanger F., Bronfman L., Dame T. M., Thaddeus P., 1998, A&A, 332, 273
Bronfman L., Alvarez H., Cohen R. S., Thaddeus P., 1989, ApJS, 71, 481
Cambrésy L., 1999, A&A, 345, 965
Chromey F. R., Elmegreen B. G., Elmegreen D. M., 1989, AJ, 98, 2203
Crane P., Lambert D. L., Sheffer Y., 1995, ApJS, 99, 107
Crawford I. A., 1991, A&A, 247, 183
Crawford I. A., 1995, MNRAS, 277, 458
Crawford I. A., 2000, MNRAS, 317, 996
Dame T. M., Hartmann D., Thaddeus P., 2001, ApJ, 547, 792
Danks A. C., Federman S. R., Lambert D. L., 1984, A&A, 130, 62
de Geus E. J., de Zeeuw P. T., Lub J., 1989, A&A, 216, 44
Diego F., 1993, Appl. Opt., 32, 6284
Diego F. et al., 1995, MNRAS, 272, 323
Federman S. R., 1982, ApJ, 257, 125
Gredel R., 1997, A&A, 320, 929
Høg E. et al., 2000, A&A, 355, L27
Houk N., 1978, Catalogue of Two Dimensional Spectral Types for the HD Stars, Vol. 2. Univ. Michigan, Department of Astronomy, Ann Arbor, MI
Houk N., 1982, Catalogue of Two-Dimensional Spectral types for the HD

Stars, Vol. 3. Univ. Michigan, Department of Astronomy, Ann Arbor, MI
Houk N., Cowley A. P., 1975, Michigan Catalogue of Two-Dimensional Spectral Types for the HD Star. Univ. Michigan, Department of Astronomy, Ann Arbor, MI
Jenkins E. B., Lees J. F., van Dishoeck E. F., Wilcots E. M., 1989, ApJ, 343, 785
Jenkins E. B., Peimbert A., 1997, ApJ, 477
Jura M., 1974, ApJ, 191, 375
Lupton R., 1993, Statistics in Theory and Practice. Princeton Univ. Press, Princeton
Mattila K., 1986, A&A, 160, 157
Mezger P. G., Mathis J. S., Panagia N., 1982, A&A, 105, 372
Mihalas D., Binney J., 1981, Galactic Astronomy: Structure and Kinematics. 2nd edn. Freeman, San Francisco, CA
Morton D. C., York D. G., Jenkins E. B., 1986, ApJ, 302, 272
Murphy D. C., Cohen R., May J., 1986, A&A, 167, 234
Nyman L.-A., Bronfman L., Thaddeus P., 1989, A&A, 216, 185
Perryman M. A. C. et al., 1997, A&A, 323, L49
Rachford B. L. et al., 2000, BAAS, 32, 1403
Rachford B. L. et al., 2001, BAAS, 33, 1049
Rachford B. L. et al., 2002, ApJ, in press
Rizzo J. R., Morras R., Arnal E. M., 1998, MNRAS, 300, 497
Sandell G., 1978, A&A, 69, 85
Savage B. D., Drake J. F., Budich W., Bohlin R. C., 1977, ApJ, 216, 291
Schwartz R. D., 1977, ApJS, 35, 161
Seidensticker K. J., Schmidt-Kaler T., 1989, A&A, 225, 192
Sofia U. J., Fitzpatrick E., Meyer D. M., 1998, ApJ, 504, L47
Spitzer L., Cochran W. D., Hirshfeld A., 1974, ApJS, 28, 373
Stothers R., Frogel J. A., 1974, AJ, 79, 456
Tachihara K., Dobashi K., Mizuno A., Ogawa H., Fukui Y., 1996, PASJ, 48, 489
van Dishoeck E. F., Black J. H., 1986, ApJS, 62, 109
Viala Y. P., 1986, A&AS, 64, 391
Vrba F. J., Marraco H. G., Strom S. E., 1992, BAAS, 24, 1246
Wannier P., Andersson B-G., Penprase B. E., Federman S. R., 1999, ApJ, 510, 291
Whittet D. C. B., Gerakines P. A., Carkner A. L., Hough J. H., Martin P. G., Prusti T., Kilkenny D., 1994, MNRAS, 268, 1
Whittet D. C. B., Prusti T., Franco G. A. P., Gerakines P. A., Kilkenny D., Larson K. A., Wesselius P. R., 1997, A&A, 327, 1194
Witt A. N., Johnson M. W., 1973, ApJ, 181, 363

APPENDIX A: A SIMPLE MODEL OF THE RADIATION FIELD AS A FUNCTION OF HEIGHT ABOVE THE GALACTIC PLANE

If we treat the Galaxy as a plane-parallel structure with stellar and dust distributions described by exponential functions (or more specifically, by hyperbolic secants) we can calculate the diffuse radiation field in the Galaxy.

To calculate the UV field for an arbitrary point, z_1, we assume that the emission and absorption coefficients, j_ν and k_ν decrease with displacement from the Galactic midplane according to scaleheights z_j and z_k. Thus,

$$j_\nu = j_\nu^{\rm o}\,\mathrm{sech}(z/z_j)$$
$$k_\nu = k_\nu^{\rm o}\,\mathrm{sech}(z/z_k). \qquad \text{(A1)}$$

We define ϕ to be the angle of rotation around the z-axis, and θ to be $\pi/2$ minus the angle with respect to the positive z-axis. Thus, the set of sightlines at $\theta = 0^\circ$ form a plane parallel to the Galactic plane, but displaced from it by z_1 (see Fig. A1). Then, taking the Galactic Plane to be infinite in extent, we find that the radiation intensity received at z_1 from all material within r' is given by

$$I_\nu(r', \theta) = \int_0^{\tau'} \frac{j_\nu}{k_\nu} \mathrm{e}^{-\tau(r,\theta)}\,\mathrm{d}\tau, \qquad \text{(A2)}$$

where

$$\tau(r, \theta) = \int_0^r k_\nu^{\rm o}\,\mathrm{sech}\left(\frac{z_1 + \rho\sin\theta}{z_k}\right)\mathrm{d}\rho$$
$$= \left[\frac{2z_k k_{\rm o}}{\sin\theta}\tan^{-1}\mathrm{e}^{\rho}\right]_{\rho=z_1/z_k}^{\rho=(z_1+r\sin\theta)/z_k}, \qquad \text{(A3)}$$

where equation (A3) simply integrates the absorptivity from the reference point at z_1 to the point (r, θ) producing the require opacity for that path-length, with ρ as a variable of integration. Changing to a spatial integration, and making use of equation (A3), equation (A2) then becomes

$$I_\nu(r', \theta) = \int_0^{r'} j_\nu^{\rm o}\,\mathrm{sech}\left(\frac{z_1 + r\sin\theta}{z_j}\right)$$
$$\exp\left(-\left\{\frac{2z_k k_{\rm o}}{\sin\theta}\left[\tan^{-1}\exp\left(\frac{z_1 + r\sin\theta}{z_k}\right)\right.\right.\right. \qquad \text{(A4)}$$
$$\left.\left.\left. \times\,\mathrm{d}r\tan^{-1}\exp\left(\frac{z_1}{z_k}\right)\right]\right\}\right)\mathrm{d}r.$$

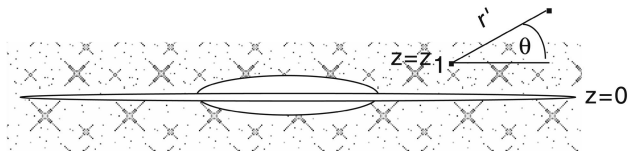

Figure A1. In order to calculate a simple model for the diffuse radiation field as a function of distance from the mid-plane, we treat the Galaxy as an infinite, plane-parallel structure. For each point z_1, the radiative transfer is integrated according to equation (A4). Note that while we have taken the artistic license of drawing a 'bulge' on the galaxy in the figure, it is not part of the plane-parallel model.

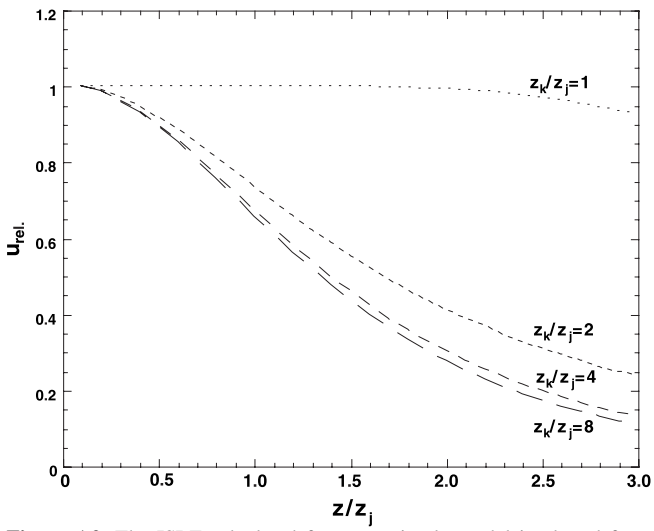

Figure A2. The ISRF calculated from our simple model is plotted for a number of parameter choices as a function of the emission scaleheight. Here four models with differing absorption scaleheights are shown. All models have been normalized to their $z/z_j = 0$ value.

The radiation density, U, resulting from all emission within a radius r' is

$$U_\nu^{r'} = \frac{1}{c}\int_{-\pi/2}^{\pi/2}\int_0^{2\pi} I_\nu(r', \theta)\cos\theta\,\mathrm{d}\phi\,\mathrm{d}\theta \tag{A5}$$

and the total radiation density, based on our assumptions, is

$$U_\nu = \lim_{r'\to\infty}\frac{2\pi}{c}\int_{-\pi/2}^{\pi/2} I_\nu(r', \theta)\cos\theta\,\mathrm{d}\theta, \tag{A6}$$

where $I_\nu(r', \theta)$ is taken from equation (A4).

Equation (A6) was evaluated numerically, by a code employing mathematical quadrature. Several tests were performed to determine the accuracy of the numerical technique, for cases where analytical limits can be calculated, in all cases producing satisfactory results.

In Fig. A2 we plot a set of model calculation results for different values of the ratio of the emission and absorption scaleheights. In Fig. 5 we have used these models together with expressions for the photodestruction of CH to compare with the observational results.

This paper has been typeset from a TEX/LATEX file prepared by the author.